Catalysis Letters (2023) 153:965–977
https://doi.org/10.1007/s10562-022-04022-2

Dual Interface Synergistic Catalysis: The Selective Hydrogenation of Crotonaldehyde Over Pt/Co_3O_4@PDA

Tong Zhang[1,2] · HuaHua Zhao[1] · Jian Yang[1] · Jun Zhao[1] · Liang Yan[1] · Lingjun Chou[1] · Huanling Song[1]

Received: 28 November 2021 / Accepted: 17 April 2022 / Published online: 20 May 2022

Abstract

Selective hydrogenation of crotonaldehyde to crotyl alcohol over PDA (polydopamine) modified Co_3O_4 supported Pt catalysts was investigated in liquid phase. The catalysts which contain PDA and Co_3O_4 lead to the formation of two kinds of interfaces: Pt-PDA and Pt-Co_3O_4, which greatly improves the performance in the hydrogenation of crotonaldehyde. TEM results reveal that the Pt nanoparticles of Pt/Co_3O_4@PDA have a smaller size and better dispersion than Pt/Co_3O_4. XPS, FT-IR and CO-DRIFTs results indicate that the addition of PDA decreases the electron density of Pt which is favor to the hydrogenation of C=O in crotonaldehyde. The characterization results demonstrate that the interaction between Pt and PDA creates new active interfacial sites and the synergy of Pt-PDA and Pt-Co_3O_4 is responsible for the excellent performance.

Graphical Abstract

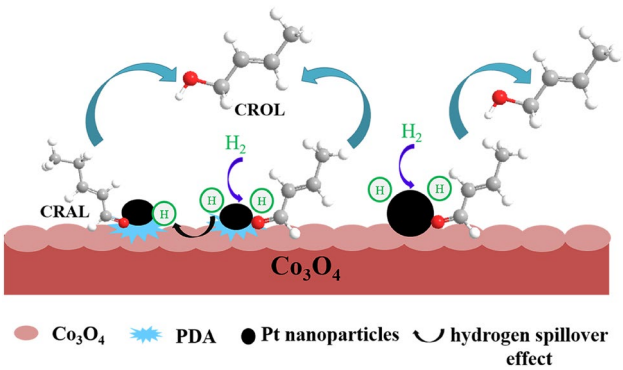

Keywords Dual interface · Synergistic catalysis · Selective hydrogenation · Crotonaldehyde

1 Introduction

Selective hydrogenation of α,β-unsaturated aldehydes to α,β-unsaturated alcohols is a pivotal tactic both in the academic research and industry applications because the unsaturated alcohols are widely used in organic synthesis, pharmaceutical industries, cosmetics and foods, which has recently attracted extensive research interest [1–3]. Usually, the hydrogenation of crotonaldehyde, one of the α,β-unsaturated aldehydes, can produce three products by selectively reducing the C=C or C=O bond, or both bonds [4], as shown in Scheme 1. However, achieving high selectivity for the desired unsaturated alcohols is challenging as

✉ Lingjun Chou
ljchou@licp.cas.cn

✉ Huanling Song
songhl@licp.cas.cn

[1] State Key Laboratory for Oxo Synthesis and Selective Oxidation, Lanzhou Institute of Chemical Physics (LICP), Chinese Academy of Sciences, Lanzhou 730000, People's Republic of China

[2] University of Chinese Academy of Sciences, Beijing 100049, People's Republic of China

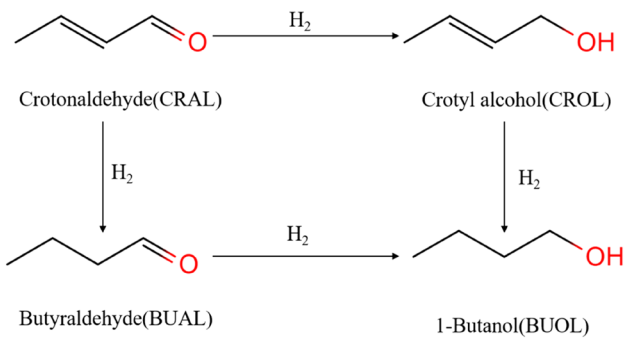

Scheme 1 Reaction pathway of crotonaldehyde hydrogenation

the hydrogenation of C=C group in reactant molecules is thermodynamically more than the C=O bond [5–7]. Traditionally, the main method of industrial production of crotyl alcohol (CROL) is to use strong reducing agents such as $LiAlH_4$ and $NaBH_4$ to reduce crotonaldehyde. Although a high yield of crotyl alcohol could be obtained by using strong reducing agents, its high energy consumption and difficult separation of products limit its applications. Instead, heterogeneous catalytic hydrogenation using H_2 as a hydrogen source is a very promising method, which is more environmentally friendly and economical than metal hydrides. Therefore, many research groups focus on supported noble metal catalysts, such as Au [8], Pt [9] and Ir [10]. However, it is difficult for these single-metal catalysts to obtain high selectivity to crotyl alcohol, so optimizing the catalyst structure is the key to improving the selectivity of crotyl alcohol.

It is well known that the adsorption mode of crotonaldehyde on the catalysts surface is closely related to the distribution of the product. The adsorption of crotonaldehyde through C=O is favor to the production of crotyl alcohol while through C=C bond leads to the formation of butyraldehyde. Therefore, in order to obtain high selectivity to crotyl alcohol, it is necessary to make crotonaldehyde mainly adsorbed through C=O double bond. Over the past decades, significant efforts have been made to improve the selectivity of crotyl alcohol. Among these, bimetallic catalysts (such as PtSn [11], PtFe [12]) and catalysts supported by reducible oxides that present the metal support interaction effect (such as Pt/TiO_2 [13], Pt/CeO_2 [14]) were proven to be effective catalysts because of structural and electronic effects. For example, Wang [15] et al. prepared PtCo/CNT bimetallic catalysts and proposed that the presence of carbon nanotubes promoted the electron transfer between Pt and Co, thus the selectivity to α,β-unsaturated alcohol was improved by changing the adsorption mode of α,β-unsaturated aldehydes. Vannice [16] et al. proposed that the metal support interfacial sites between Pt and TiO_2 can improve the selectivity to crotyl alcohol by polarizing C=O bond of substrates. In addition, the selectivity of unsaturated alcohols can also be improved by adding a promoter to the catalyst to design a suitable interface. For example, Ir-MoO_x/BN catalysts presented high selectivity for crotyl alcohol due to the formation of Ir-MoO_x interfacial sites, which is favor to adsorb crotonaldehyde through C=O bond. Such strategy of designing new interfacial sites has been studied in many systems [17–22].

In the present work, novel polydopamine (PDA) modified Co_3O_4 nanoparticles (named Co_3O_4@PDA) were successfully synthesized and Co_3O_4@PDA nanoparticles were impregnated with Pt to prepare the Pt/-Co_3O_4@PDA catalysts. The selective hydrogenation of crotonaldehyde in liquid phase was chosen as the model reaction and the catalytic performance of the modified catalysts was compared with Pt/Co_3O_4. The catalytic performance shows that Pt/Co_3O_4@PDA exhibits excellent selectivity for crotyl alcohol. The characterization results reveal that Pt/Co_3O_4@PDA contains two kinds of interfaces: Pt-PDA and Pt-Co_3O_4, which are responsible for the enhanced performance.

2 Experimental

2.1 Materials

Chloroplatinic acid hexahydrate ($H_2PtCl_6{\cdot}6H_2O$) was purchased from the Sinopharm Chemical Reagent Co., Ltd., China. Dopamine (DA) hydrochloride was provided by Aladdin Co., Ltd., China. Hydrochloric acid (HCl), cobalt oxide (CoO) and trometamol ($C_4H_{11}NO_3$) were purchased from Chengdu Kelong Chemical Co., Ltd., China. Ethylene glycol ($C_2H_6O_2$), absolute ethanol (C_2H_5OH), crotonaldehyde, cinnamaldehyde, furfural, and methacrylaldehyde were purchased from Tianjin Bohua Chemical Reagent Co., Ltd., China.

2.2 Synthesis of Co_3O_4@PDA Nanoparticles

As previously reported in the literature dopamine can self-polymerize and deposit polydopamine on the surface of many materials such as TiO_2, Al_2O_3 in basic solution [23]. In a typical synthesis, Co_3O_4 was prepared by heating CoO to 400 °C at a ramp rate of 5 °C /min and kept for 2 h in the muffle furnace. Then 0.5 g Co_3O_4 nanoparticles were dispersed in 15 mL Tris–HCl (pH 8.5) solution by magnetic stirring for 10 min to form a suspension. Subsequently, 30 mg dopamine was added to the mixture under stirring to form 2 g/L dopamine mixture. The mixture was subjected to continuous magnetic stirring at ambient temperature for 24 h. Afterwards, the precipitates were collected by centrifugation, then washed four times with deionized water and one time with ethanol. Finally, the composite was dried at 65 °C in vacuum oven for 12 h and denoted

as Co_3O_4@6wt%PDA (6wt% is the mass ratio of dopamine to Co_3O_4). The Co_3O_4@4wt%PDA, Co_3O_4@8wt%PDA and Co_3O_4@10wt%PDA were prepared in the similar method by changing the amount of Tris–HCl solution and dopamine.

2.3 Synthesis of Pt-Based Catalysts

The supported Pt/Co_3O_4@6wt%PDA catalyst was prepared by impregnating Co_3O_4@6wt%PDA with the ethanol solution of $H_2PtCl_6{\cdot}6H_2O$. In detail, 0.25 g Co_3O_4@6wt%PDA was added to the 6 mL 1.85 g/L ethanol solution of $H_2PtCl_6{\cdot}6H_2O$ in 25 mL round flask. Then the suspension was stirred 30 min and maintained for 24 h at room temperature, thereafter the excessive solvent was removed by evaporated at 80 °C. Arter cooling to room temperature, 4 mL ethylene glycol was added to the round flask and heated to 80 °C kept 10 min then heating to 110 °C and reflux condensation for 4 h. Afterwards, the catalysts were collected by centrifugation and washed four times with deionized water and one time with ethanol. Finally, the composite was dried at 65 °C in vacuum oven for 12 h and denoted as Pt/Co_3O_4@6wt%PDA. The Pt/Co_3O_4, Pt/Co_3O_4@4wt%PDA, Pt/Co_3O_4@8wt%PDA and Pt/Co_3O_4@10wt%PDA were prepared in the similar way by changing the support.

2.4 Catalyst Characterizations

Transmission electron microscopy (TEM) images and selected area electron diffraction (SAED) were performed on the TECNAI G2 F20 high-resolution transmission electron microscopy under a working voltage of 200 kV. Filed emission scanning electron microscopy (FESEM) was performed on the HITACHI SU8020 microscopy.

X-ray diffractograms (XRD) measurements were carried out on an X'Pert Pro Multipurpose diffractometer (PANalytical, Inc.) with Ni-filtered Cu Kα radiation (0.15406 nm) from 10° to 80° operated at 40 kV and 20 mA. Nitrogen adsorption and desorption isotherms of samples were recorded on an Anton Paar analyzer (Quantachrome Instruments U.S.) at 77 K. The specific surface area was calculated via the Brunauer–Emmett–Teller (BET) method. Prior to test, the samples were degassed at 180 °C for 2 h.

X-ray photoelectron spectroscopy (XPS) of the samples were performed on a Thermo Scientific ESCALAB250xi spectrometer. All binding energy (BE) values were referenced to the C1s peak of contaminant carbon at 284.8 eV with an uncertainty of ± 0.2 eV. The thermogravimetric-differential scanning calorimetry (TG-DSC) analyses of samples were performed on a NETZSCH STA 449F3 thermogravimetric analyzer from room temperature to 800 °C with a ramping rate of 10 °C/min under air atmosphere.

H_2-TPD measurements were performed on using a ChemBET Pulsar TPR/TPD analyzer with a mass detector (LC-D200M). 200 mg of catalysts were pretreated at 200 °C in He flow (30 mL/min) for 1 h prior to analysis, thereafter they were cooled to 25 °C. After that, He was replaced by 7% H_2 in Ar (30 mL/min), the temperature was raised to 70 °C and maintained for 1 h. Subsequently, the H_2 desorption peaks were collected under He gas (30 mL/min) at a ramp rate of 10 °C/min to 900 °C after the mass spectrometer signal stabilized.

The FT-IR studies were performed using a Nicolet iS50 FT-IR spectrometer. Diffuse reflectance infrared Fourier transform (DRIFT) spectra of CO chemisorption on the catalysts were recorded using an FT-IR spectrometer (Nicolet iS50) equipped with a MCT detector and a PIKE DRIFT accessory. Prior to the measurement, the catalysts were pretreated in a N_2 flow (20 mL/min) at 150 °C for 60 min. Then the samples were cooled down to 40 °C and the backgrounds were collected. After that, the samples were exposed to a 10% CO in N_2 (20 mL/min) for 30 min and purged by N_2 flow for another 30 min. The spectra were recorded with subtracted the background at the corresponding time. In all cases the spectra were taken with a resolution of 4 cm^{-1} and cumulative 64 scans.

The Pt content analysis of different catalysts was performed using an inductively coupled plasma-optical emission spectrophotometer (ICP-OES, Thermo Electron IRIS Intrepid II XSP, USA).

2.5 Catalytic Hydrogenation

The hydrogenation of crotonaldehyde in liquid phase was performed in a 25 mL high-pressure autoclave with magnetic stirrer. For a typical catalytic hydrogenation, 0.02 g of catalysts and 0.1 mL of crotonaldehyde were added in 5 mL of ethanol. Then the autoclave was purged four times with hydrogen. After that, the reaction was performed in the reactor charged with 2.0 MPa H_2 at 70 °C for 1 h with vigorous stirring at 500 rpm. Finally, the products were separated by centrifugation and analyzed by GC–MS. The conversion (Conv.) of crotonaldehyde and selectivity (Sel.) of products were defined as follows:

$$\text{Conv. } (C_4H_6O) = \frac{n C_4H_6O_{(0)} - n C_4H_6O_{(i)}}{n C_4H_6O_{(0)}} \times 100\% \quad (1)$$

$$\text{Sel. (X)} = \frac{n_x}{n C_4H_6O_{(0)} - n C_4H_6O_{(i)}} \times 100\% \quad (2)$$

where $nC_4H_6O_{(0)}$ and $nC_4H_6O_{(i)}$ are the moles of the initial and residual crotonaldehyde, respectively. The n_x was the mole of the product.

3 Results

3.1 X-Ray Diffraction

The XRD patterns of the synthesized Co_3O_4, Pt/Co_3O_4, Co_3O_4@6wt%PDA and Pt/Co_3O_4@PDA are shown in Fig. 1a. A series of diffraction peaks located at 19°, 31.27°, 36.85°, 44.81°, 59.35° and 65.23° were observed in the XRD patterns of all samples. These peaks correspond to the (111), (220), (311), (400), (511) and (440) planes of cobalt oxide crystals (JCPDS No. 43-1003), respectively [24]. However, no typical diffraction peaks of Pt species were observed over supported Pt catalysts, demonstrating that the Pt species are highly dispersed on the catalysts surface owing to low Pt addition.

3.2 Nitrogen Adsorption–Desorption Isotherms and ICP

N_2 adsorption–desorption characterization was performed to measure porosity of catalysts and the results are shown in Fig. 1b and Table 1. As shown, the samples presented the typical type-IV isotherm with hysteresis loops, which indicated that the catalysts contain mesoporous structure. The BET surface area of the synthesized catalysts gradually increased from 17.4 m^2/g of Pt/Co_3O_4 to 47.0 m^2/g of Pt/Co_3O_4@10wt%PDA with the increase of dopamine input, as shown in Table 1. It was reported that the polydopamine can present the intrinsic pore structure with the main pore size ranging from 1.7 to 5.5 nm [25]. Therefore, the modified catalyst may have more pores leading to the specific surface area increased deriving from PDA coating on Co_3O_4. In addition, all samples showed the similar average pore size and gentle volcano-type change of pore volume as PDA increasing. Moreover, the content of Pt in catalysts was tested by ICP analysis, as shown in Table 1, which were well controlled between 1.0 and 1.3%.

3.3 SEM and TEM

Scanning electron microscopy (SEM) images of Co_3O_4 and Co_3O_4@6wt%PDA showed that the particles were generated from the agglomeration of smaller particles

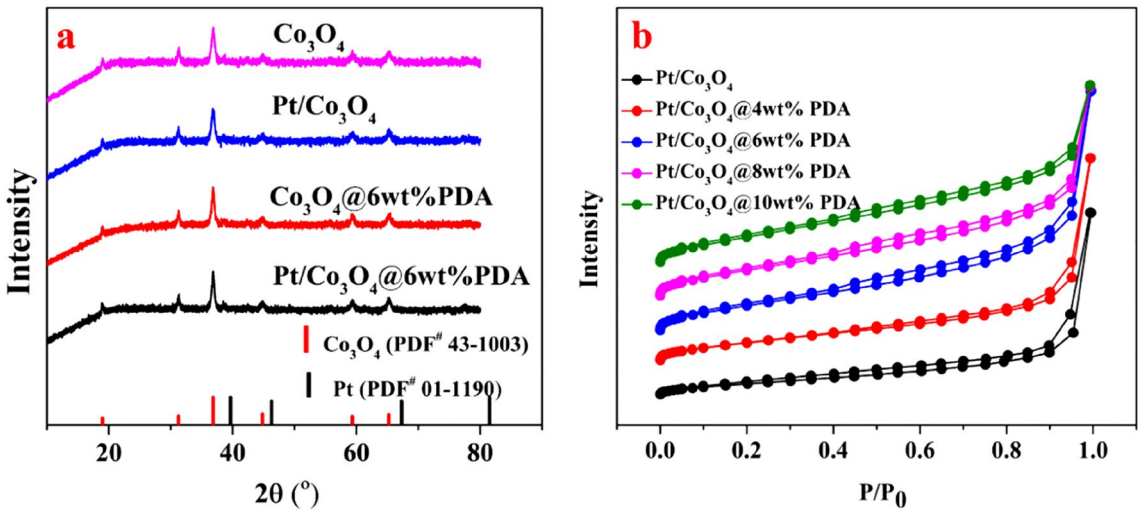

Fig. 1 XRD patterns of different samples (**a**), N_2 adsorption–desorption isotherms of samples (**b**)

Table 1 Physicochemical parameters of the catalysts made in this study

Catalyst	S_{BET} (m^2/g)	V p (cm^3/g)	D p (nm)	Pt loading (wt%)	Content of Pt species (%)[a]	
					Pt^0	$Pt^{\delta+}$
Pt/Co_3O_4	17.4	0.091	1.7	1.1	61.8	38.2
Pt/Co_3O_4@4wt%PDA	30.5	0.102	1.7	1.2	57.2	42.8
Pt/Co_3O_4@6wt%PDA	41.6	0.118	1.7	1.0	42.6	57.4
Pt/Co_3O_4@8wt%PDA	44.9	0.104	1.7	1.1	40.3	59.7
Pt/Co_3O_4@10wt%PDA	47.0	0.087	1.7	1.3	38.8	61.2

[a]Calculated by XPS

and the SEM images of Co_3O_4 were similar to those of Co_3O_4@6wt%PDA, indicating that Co_3O_4 morphology was maintained during modification (Fig. 2a, b). Transmission electron microscopy (TEM) images of samples with different amounts of PDA showed that Pt nanoparticles of the modified catalysts have better dispersibility and smaller particle

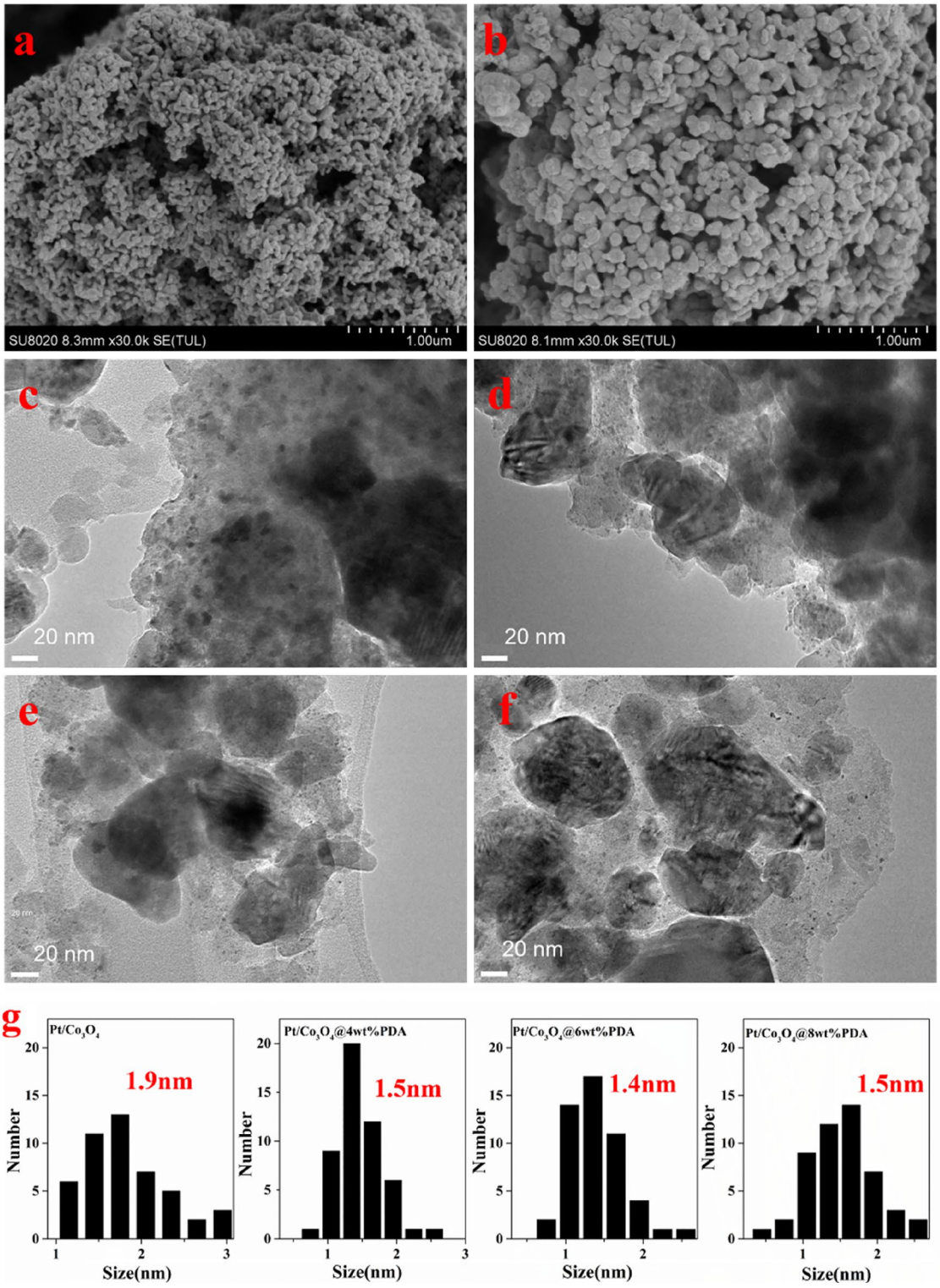

Fig. 2 SEM images of Co_3O_4 (**a**), Co_3O_4@6wt%PDA (**b**) and TEM of Pt/Co_3O_4 c), Pt/Co_3O_4@4wt%PDA (**d**), Pt/Co_3O_4@6wt%PDA (**e**), Pt/Co_3O_4@8wt%PDA (**f**), the Pt particle sizes distribution of each samples (**g**)

size (Fig. 2d–f, ~ 1.5 nm) than the unmodified (~ 1.9 nm) catalyst (Fig. 2c). This is mainly because the nitrogen-containing functional groups of PDA exhibited an excellent metal-binding ability for absorbing $PtCl_6^{2-}$ ions onto the surface of the support [26], which is favor to the dispersion of Pt nanoparticles.

The HRTEM image of Pt/Co_3O_4@6wt%PDA showed the oriented and ordered fringe pattern. The d-spacing value of 0.24 nm is consistent with that of Co_3O_4(111) planes. Furthermore, the EDS mappings of the Pt/Co_3O_4@6wt%PDA were also investigated, as shown in Fig. 3b, and suggested that the elements of Pt, O, C, Co, and N distribute homogeneously within the microsphere. In addition, the existence of N indicated that PDA modified the Co_3O_4 successfully. Comparing these mappings carefully, it can be seen that Pt might interact with PDA besides Co.

3.4 TG-DSC

In order to confirm the actual amount of PDA in different catalysts, thermogravimetric analysis was performed. As shown in Fig. 4, a weight loss below 200 °C is attributed to the removal of the impurities such as adsorbed water or gas molecules. It is worth noting that a major weight loss takes place between 200 and 310 °C which can be attributed to the thermal decomposition of polydopamine for all samples. At the same time, an accompanying exothermal peak was enhanced with the increase of PDA from 4 to 10% in the sample. The corresponding weight loss from 3.3 to 7.7% was close to the theoretical value.

3.5 H_2-TPD

H_2-spillover plays an important role in the hydrogenation reactions by increasing the availability of adsorbed H_2 on the catalyst surface, which can facilitate the hydrogenation of substrates. H_2-TPD was performed to distinguish the characteristics of the catalysts containing different PDA amounts. As shown in Fig. 5, the H_2-TPD profiles present high temperature (> 400 °C) and low temperature (< 400 °C) desorption regions. The Pt/Co_3O_4 catalyst only exhibits one H_2 desorption peak in the low temperature regions at the top of 310 °C, whereas the Pt/Co_3O_4@6wt%PDA presents two H_2 desorption peaks in the low temperature regions at the top of 270 °C, 340 °C and one desorption peak in the high temperature regions at the top of 420 °C. Similarly, high temperature H_2 desorption peaks appear in Pt/Co_3O_4@4%PDA and Pt/Co_3O_4@8%PDA, as shown in Fig. S1. Furthermore, the decomposition of PDA at this region was excluded through control test. In general, weak hydrogen adsorption on the catalyst presents low temperature desorption peaks, whereas high temperature desorption peaks are attributed to spillover or subsurface hydrogen adsorption [27–29]. Thus, the PDA modified catalysts increase both weak H_2 adsorption sites and strong H_2 adsorption sites which may facilitate the hydrogenation of crotonaldehyde.

3.6 XPS

The electronic state of metal nanoparticles has a great influence on the catalytic performance of α,β-unsaturated aldehyde selective hydrogenation to α,β-unsaturated alcohol [30–32]. XPS was applied to characterize the surface electron density of Pt and N atoms in PDA modified Co_3O_4 supported Pt catalysts. As shown in Fig. 6a and Fig. S2, Pt $4f_{7/2}$ spectra can be resolved into two components at BEs of 71.3–71.5 eV and 72.1–72.9 eV, attributed to metallic Pt^0 and oxidized $Pt^{\delta+}$ species, respectively [33–36]. The results showed that after the PDA promotion the BEs of the metallic Pt^0 shift to higher values by 0.2–0.4 eV and the BEs of the oxidized $Pt^{\delta+}$ shift to higher values by 0.8 eV, demonstrating the interaction between Pt and PDA. The N1s spectrum is composed of two subpeaks at BEs of 399.1–399.4 eV and 400.2–400.4 eV corresponding to pyridinic and pyrrolic N

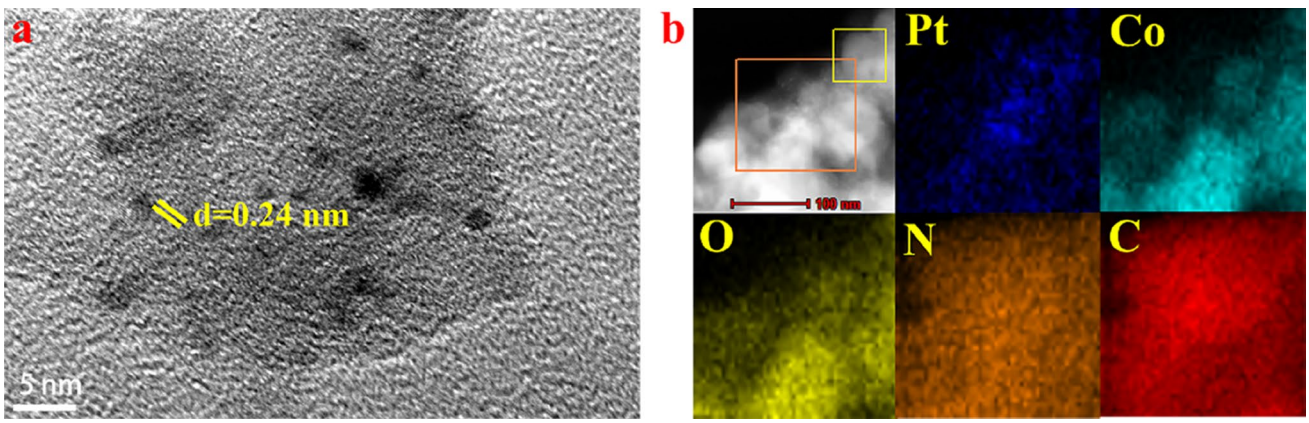

Fig. 3 HRTEM image and corresponding elemental mappings of Pt/Co_3O_4@6wt%PDA (The scale bar of image a is 5 nm)

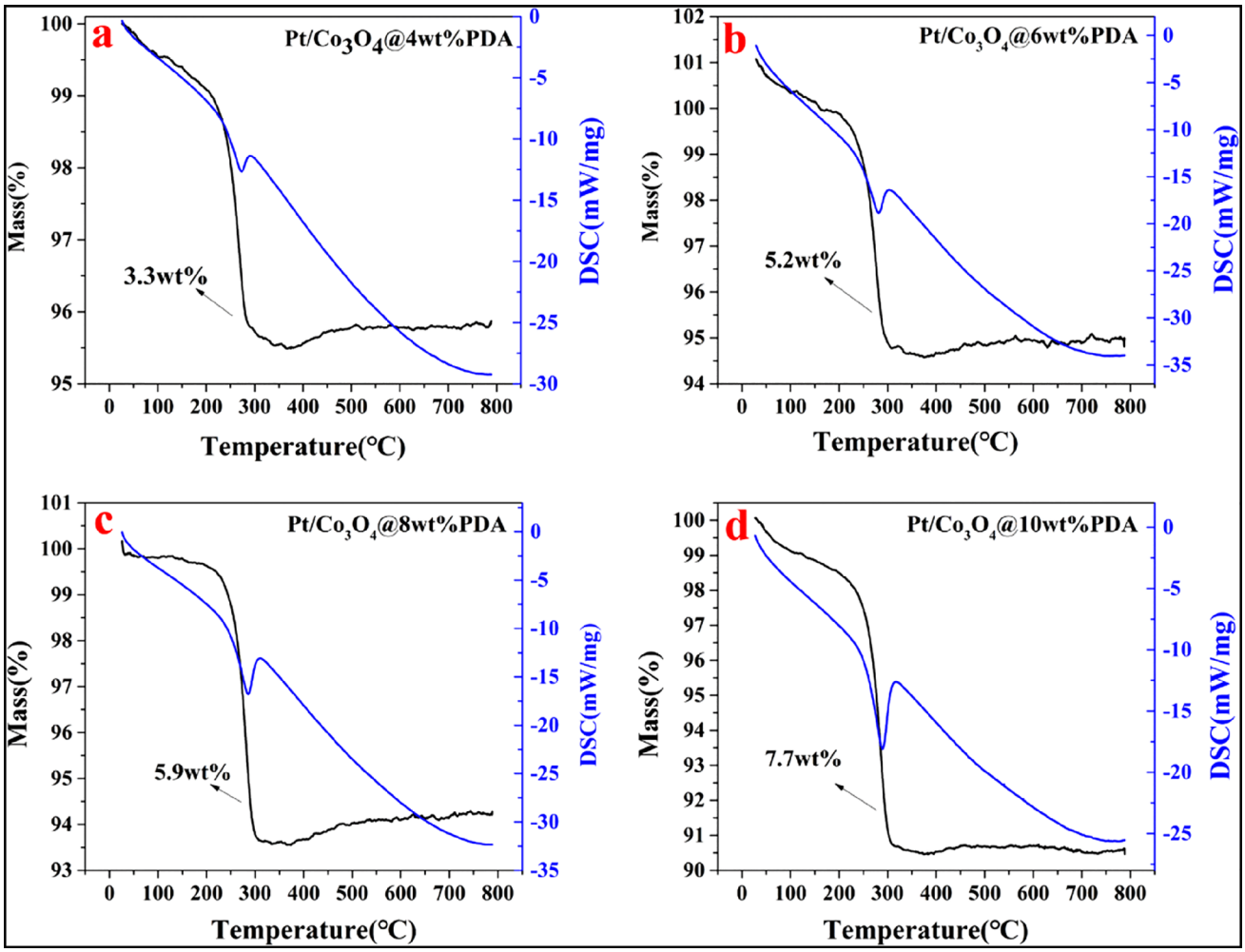

Fig. 4 TG and DSC of Co_3O_4@4wt%PDA (**a**), Co_3O_4@6wt%PDA (**b**), Co_3O_4@8wt%PDA (**c**), Co_3O_4@10wt%PDA (**d**)

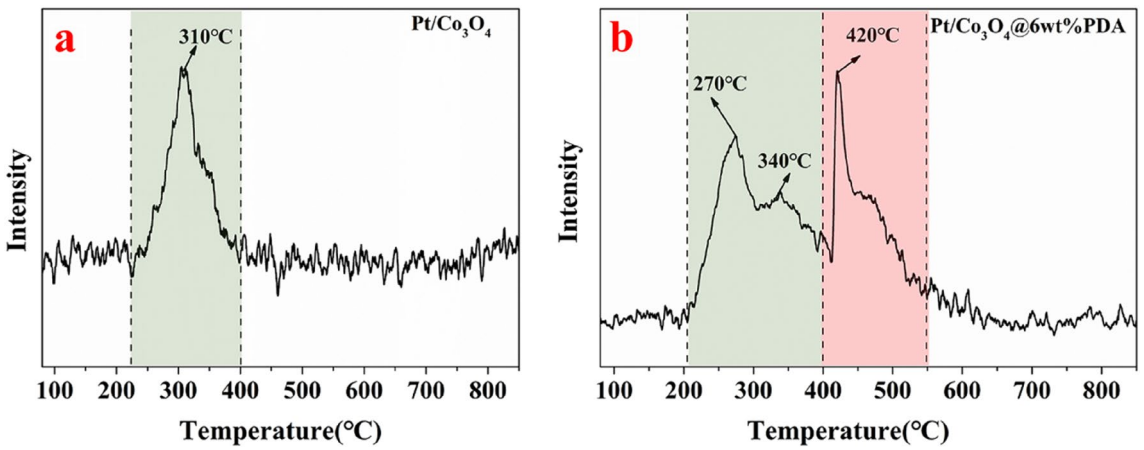

Fig. 5 H_2-TPD profiles of Pt/Co_3O_4 (**a**), and Pt/Co_3O_4@6wt%PDA (**b**) of mass spectrometry signal

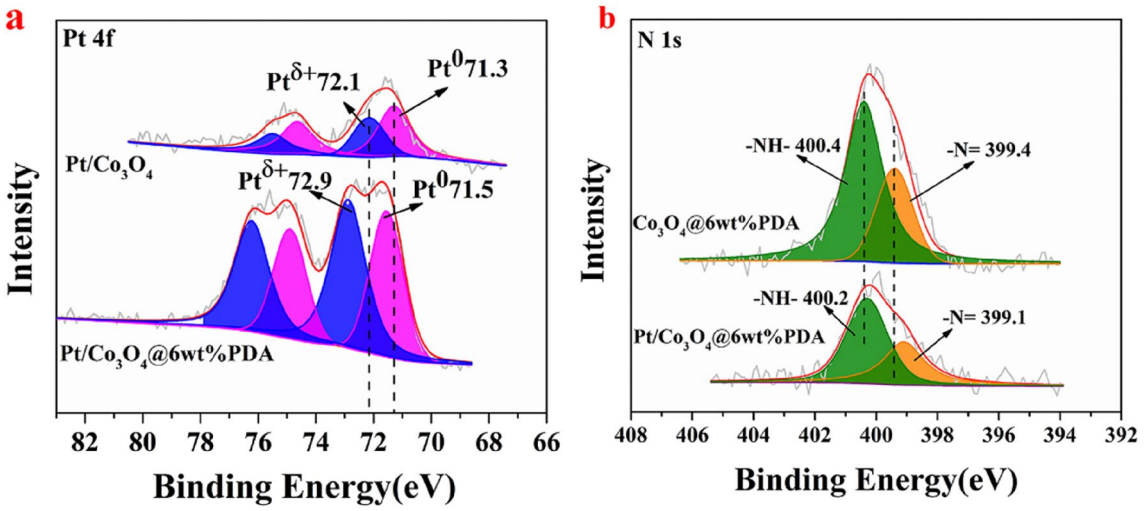

Fig. 6 XPS profiles of different catalysts of Pt 4f (**a**), N 1 s (**b**)

species, respectively [37, 38]. The BEs of pyridinic and pyrrolic N slightly shift to lower valves by 0.2–0.3 eV after supported Pt, which indicates the charge transfer from Pt to PDA. In addition, with the increase of PDA amount to 10 wt%, the fraction of surface $Pt^{\delta+}$ species (determined by XPS) increased from 38.2 to 61.2%, shown in Table 1.

3.7 FT-IR

In order to further investigate the interaction between Pt and N groups FT-IR was conducted. As shown in Fig. 7a in the Co_3O_4@6wt%PDA spectrum, a new peak at 1498 cm^{-1} emerged in comparison with Co_3O_4 which can be ascribed to the shearing vibration of N–H groups in PDA [39]. It is well known that the Pt–N interaction can cause a shift of N–H wavenumber [40]. In fact, a blue shift of N–H vibration peak to 1507 cm^{-1} can be observed after Pt was loaded on Co_3O_4@6wt%PDA, which indicated that N–H bond was weakened and the electron charge transferred from Pt to N groups, similar to the XPS results.

3.8 CO-DRIFTs

In order to further probe the electronic states of the Pt species in the catalysts CO-DRIFTS experiments were performed. As shown in Fig. 7b and Fig. S3, evacuation with time leads to the gradual disappearance of gas phase CO absorbed at 2170 cm^{-1} [41]. The Pt/Co_3O_4 catalyst only presents one peak at ~ 2070 cm^{-1} after N_2 evacuated 30 min which can be attributed to CO linearly adsorbed on Pt^0 [42].

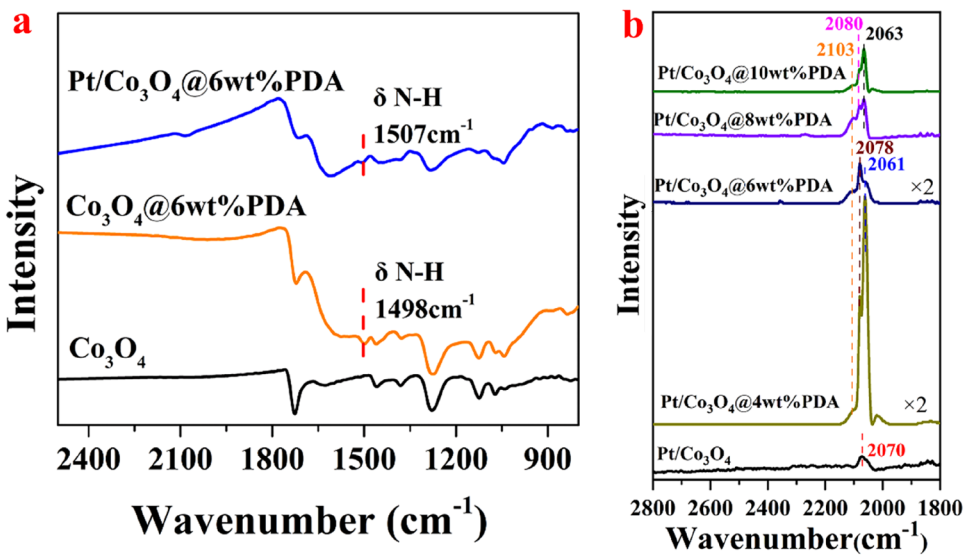

Fig. 7 FT-IR (**a**) and CO-DRIFTs (**b**) of different catalysts

Whereas, the PDA modified catalysts display three peaks at ~ 2061 cm^{-1}, ~ 2080 cm^{-1} and ~ 2103 cm^{-1} which can be assigned to CO linearly adsorbed on smaller Pt^0 [43], lower electron density Pt^0 and oxidized $Pt^{\delta+}$ [44], respectively. It is known that small particles possess low Pt coordination and CO adsorption on these sites presents lower wavenumbers, and the stretching frequency of CO adsorbed on a metal surface is also sensitive to the surface electron states of Pt by affecting the back donation of electrons from Pt to the antibonding 2π-orbitals of adsorbed CO [42]. Indeed, the electronic properties and the structure of Pt have been modified by the addition of PDA. Thus, both red shift and blue shift can be observed in Fig. 7b comparing Pt/Co_3O_4 and $PtCo_3O_4$@PDA implying the strong interaction between Pt and N groups which created smaller Pt nanoparticles and lower electron density Pt nanoparticles, consistent with TEM, FT-IR and XPS.

3.9 Catalytic Performance

In order to evaluate the catalytic performance of Pt/Co_3O_4 and Pt/Co_3O_4@PDA, the hydrogenation of crotonaldehyde was performed at 70 °C, 2 MPa H_2 and 1 h. As shown in Fig. 8, the Pt/Co_3O_4 and the series of Pt/Co_3O_4@PDA catalysts with PDA content from 4 to 8wt% presented similar conversions. However, when the PDA content was further increased to 10wt% the conversion of crotonaldehyde declined. Regarding the selectivity, the Pt/Co_3O_4 catalyst delivered a 47.8% selectivity to the crotyl alcohol, which caused by the metal support interaction effect between Pt and Co_3O_4. After adding PDA to the catalyst, the selectivity to crotyl alcohol gradually increases and reaches a maximum (69.9%) at the PDA content of 6wt% (Pt/Co_3O_4@6wt%PDA) which indicate that the modification of PDA is more favorable for C=O hydrogenation than C=C. When further increased the PDA content to 10 wt% the selectivity to crotyl alcohol was reduced to 53.8% caused by more others formation (7.2wt%, such as C_8 compounds formed by polymerization). In addition, the rate of crotyl alcohol formation also reaches a maximum (1757 mmol g^{-1}Pt h^{-1}) at the PDA content of 6wt% (Pt/Co_3O_4@6wt%PDA), as shown in Table S1. Furthermore, the Pt/SiO_2 and Pt/SiO_2@4wt%PDA were also prepared and evaluated as control catalysts. The Pt/SiO_2 and Pt/SiO_2@4wt%PDA exhibited the higher conversion but a lower selectivity to crotyl alcohol compared with Pt/Co_3O_4 and Pt/Co_3O_4@PDA catalysts. This is mainly because the SiO_2 is an inert support and has no impact on the catalytic reactions occurring on the Pt nanoparticle surface [45]. Interestingly, Pt/SiO_2@4wt%PDA delivered the highest conversion of 100% but no crotyl alcohol product which implied the role of H_2 spillover caused by the interface of Pt-PDA.

In addition, the effects of reaction temperature, time and pressure were also investigated over Pt/Co_3O_4@6wt%PDA. As shown in Fig. 9a, with the temperature increases the conversion of crotonaldehyde increases from 26.9 (30 °C) to 75.5% (100 °C). However, the selectivity to crotyl alcohol declines from 72.6 (30 °C) to 42.7% (100 °C) due to the over hydrogenation generating more 1-butanol [46], which suggest that at a relatively low temperatures Pt/Co_3O_4@6wt%PDA catalyzed hydrogenation of C=O is more favorable than that of C=C. With increasing reaction time from 1 to 5 h the conversion of crotonaldehyde increased from 41.4 to75.9%, nevertheless selectivity to crotyl alcohol slightly decreased from 69.9 to 61.9%. The effect of H_2 pressure was then evaluated under 70 °C and 1 h. As shown in Fig. 9c, increasing H_2 pressure from 1 to 3 MPa leads to an increase in crotonaldehyde conversion from 31.6 to 53.9%. Furthermore, the selectivity to crotyl alcohol increased slightly from 67.1 to 69.9% and decreased to 64.5% with further increased H_2 pressure to 3 MPa caused by the over hydrogenation of crotonaldehyde to form1-butanol. More importantly, the formation rate of crotyl alcohol enhanced

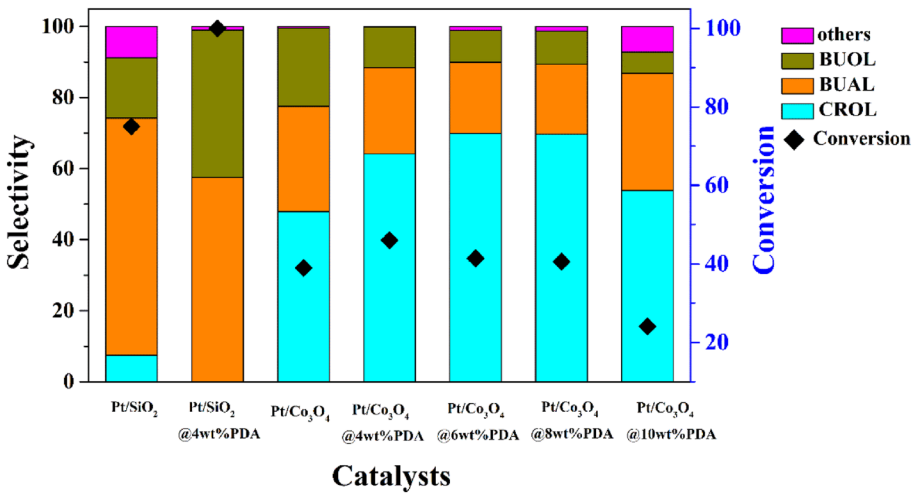

Fig. 8 Catalytic performance over different catalysts. Reaction conditions: crotonaldehyde (0.1 ml), ethanol (5 ml), catalysts (0.02 g), 1 h, 2 MPa H_2, 70 °C

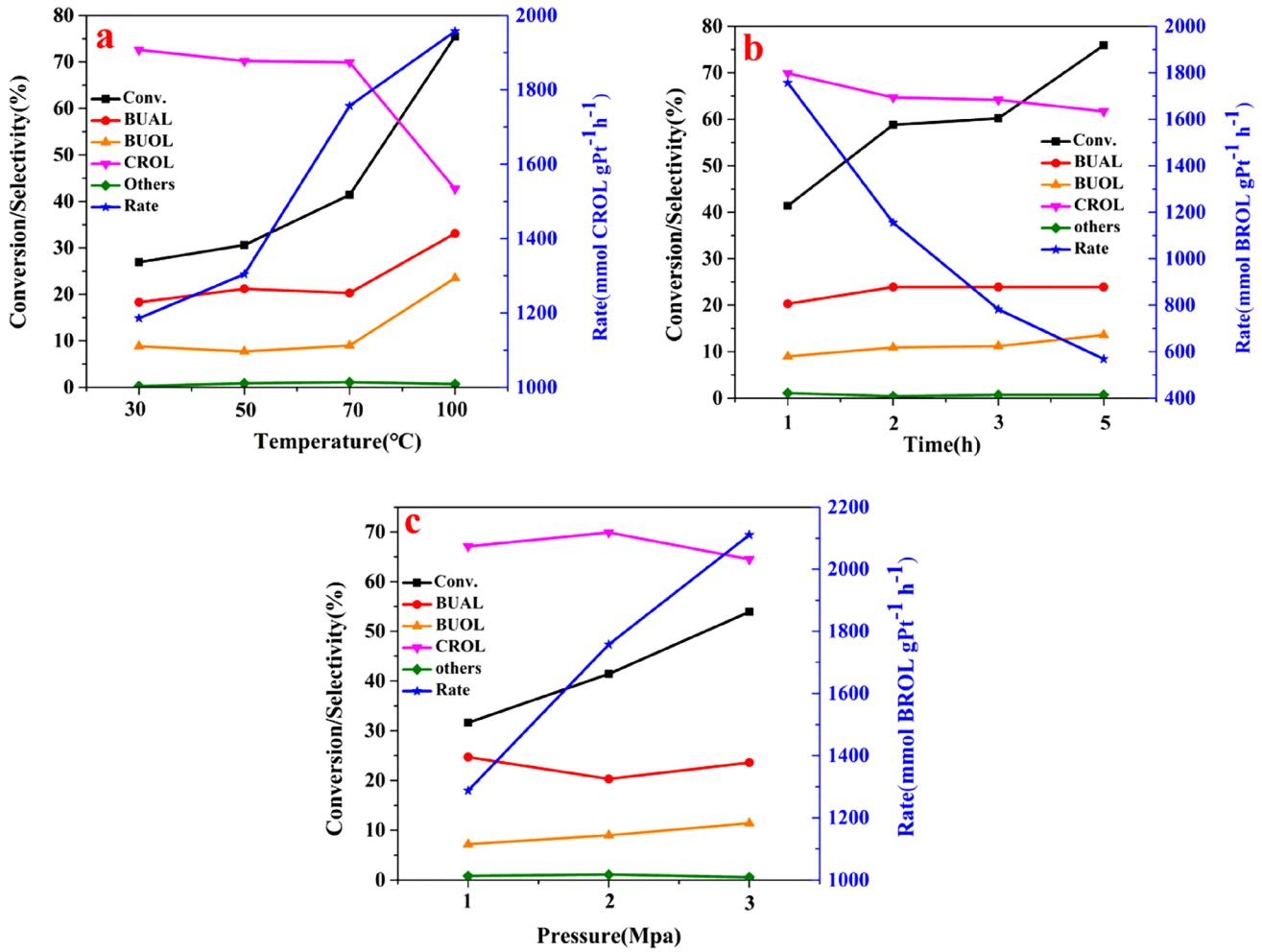

Fig. 9 Effect of reaction temperature (1 h, 2 MPa H_2) (**a**), reaction time (70 °C, 2 MPa H_2 (**b**), H_2 pressure (70 °C, 1 h) (**c**) on Pt/Co_3O_4@6wt%PDA catalyzed selective hydrogenation of crotonaldehyde to crotyl alcohol. Reaction conditions: crotonaldehyde (0.1 ml), ethanol (5 ml), catalysts (0.02 g)

constantly as crotonaldehyde conversion increased under fixing reaction time even as high as 2100 mmol·g^{-1} Pt·h^{-1} or more (Fig. 9c), which suggested that the selective hydrogenation of crotonaldehyde was effectively promoted over Pt/Co_3O_4@6wt%PDA. The comparative experiment of Pt/Co_3O_4, Pt/Co_3O_4@6wt%PDA and Pt/Co_3O_4@8wt%PDA at 70 °C, 2Mpa H_2 and 2 h was carried out (Table S2) to further distinguish the catalytic performance. It can be seen that the conversion increased by about 10% and the selectivity just decreased by about 3% for Pt/Co_3O_4 compared with 1 h. In addition, the crotyl alcohol selectivity of Pt/Co_3O_4@8wt%PDA suffered from a serious decline by comparing with 1 h owing to forming more non-hydrogenation byproduct although the conversion increased greatly.

Considering the excellent performance of Pt/Co_3O_4@6wt%PDA, the selective hydrogenation reaction of other α,β-unsaturated aldehydes to form corresponding unsaturated alcohols was also studied, and the results are presented in Table 2. It is found that Pt/Co_3O_4@6wt%PDA is more favorable for C=O hydrogenation to form unsaturated alcohol for a series of substrates. For example, the selectivity to cinnamyl alcohol reached to 94% at cinnamaldehyde conversion of 78%. Moreover, the selectivity of > 99.9% for C=O bond in furfural was obtained. The difference in conversion and selectivity of α,β-unsaturated aldehydes hydrogenation is mainly concerned with the molecular structure of substrate. A larger substituent is favorable to enhance the selectivity of C=O hydrogenation through changing the adsorption model because the steric effect can hinder C=C adsorption [47–49]. Hence, the cinnamaldehyde and furfural exhibted higher selectivity of unsaturated alcohols, while methacrylaldehyde with smaller substituent shows a similar selectivity to crotonaldehyde. Whereas, the conversion rate is related to adsorption strength of reactant molecule, which is affected by the above structural factors to some extent.

Table 2 Selective hydrogenation of other unsaturated aldehydes over Pt/Co_3O_4@6wt%PDA

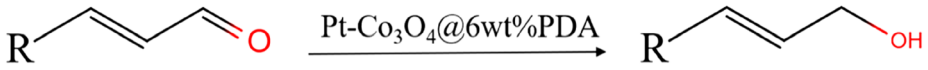

Entry	Substrate	Product	Conversion	Selectivity
1	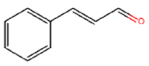	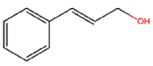	78.5%	94.1%
2		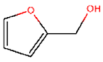	39.7%	> 99.9%
3	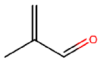	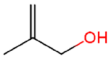	41.6%	65.3%

Reaction conditions: substrates (0.1 ml), ethanol (5 ml), catalysts (0.02 g),1 h, 2 MPa H_2, 70 °C

4 Discussion

Over past decades, many efforts have been made to increase the selectivity to unsaturated alcohol. It is well known that adding second metals (such as Sn, Fe) to catalyst formed bimetal catalysts can improve the selectivity to unsaturated alcohols through changing the electron density of primary metals which is favor to adsorb C=O bond [50, 51]. In addition, the reducible metal oxides supported catalysts also have relatively higher selectivity to unsaturated alcohols due to the metal support interaction which can form metals/MO_x interface sites for activation of C=O bond [52, 53]. For Pt based catalysts, the effect of Pt size on the selective hydrogenation performance of α,β-unsaturated aldehyde seems unusual. It was observed that the selectivity to the unsaturated alcohol increased with increasing Pt particle sizes because the larger Pt particles expose more Pt (111) surfaces which is favor to the adsorption of crotonaldehyde via the C=O bond [54] but requires a large range of particles sizes [30]. Zhu found that the selectivity appeared to be independent of the Pt particle sizes, due to the sizes only ranged from 1.5 to 2.5 nm in their work [55].

In this work, the hydrogenation of crotonaldehyde was carried out in the liquid phase over Pt/Co_3O_4, series of Pt/Co_3O_4@PDA, Pt/SiO_2 and Pt/SiO_2@4wt%PDA catalysts. Compared Pt/Co_3O_4 with Pt/Co_3O_4@PDA (TEM in Fig. 2), Pt particle sizes decreased from ~ 1.9 to ~ 1.5 nm after the addition of PDA which has barely influence in the selectivity to unsaturated alcohol. Thus, the electronic environment of surface Pt nanoparticles was focused. As well known, electron density of Pt active sites greatly affect H_2 activation, and the ability of activating hydrogenation will be weaken when the electron density decreases [56].

Interestingly, series of Pt/Co_3O_4@PDA showed higher activity than Pt/Co_3O_4 catalysts even though the lower Pt electron density existed in the former by XPS and CO-DRIFTS characterizations. It could be closely connected with H_2 spillover phenomenon in the presence of Pt/Co_3O_4@PDA catalysts evidenced by H_2-TPD which will facilitate the hydrogenation process. Moreover, the hydrogenation of crotonaldehyde performance over Pt nanoparticles supported on inert SiO_2 (Pt/SiO_2) and Pt/SiO_2@4wt%PDA demonstrated that the conversion increased from 75 to 100% after the addition of PDA and butanol selectivity enhanced greatly (Table S1). This promotion of hydrogenation activity might be attributed to H_2 spillover. However, it has been reported that PDA contains phenolic hydroxyl group which can act as Lewis acid sites promoted the occurrence of side reactions [23], thus it is reasonable that the excess PDA (Pt/Co_3O_4@10wt%PDA) could give rise to the increase of the acetal-like byproducts (Fig. 8).

Co_3O_4 as a reducible support, an important issue to take into account is the interaction between Pt and oxide support for the selectivity to C=O bond hydrogenation. As the previous reported, Pt supported on reducible metal oxides usually improves the unsaturated alcohol selectivity owing to their electron transfer interaction [13, 14]. The same results were obtained in our research. For instance, Pt/SiO_2 and Pt/SiO_2@4wt%PDA catalysts showed poor selectivity to crotyl alcohol, but it is significantly enhanced to 47.8% over the Pt/Co_3O_4 catalysts, which exactly attributed to Co_3O_4 interacting with Pt and forming Pt-Co_3O_4 interface sites so as to the preferential adsorption of C=O bond.

After adding PDA to Pt/Co_3O_4 catalysts, the selectivity towards crotyl alcohol further increase to 69.9%(Pt/Co_3O_4@6wt%PDA) due to new active sites Pt-PDA formed by the interaction between Pt nanoparticles and amine groups. Albeit Pt 4f binding energy shift in XPS and the migration of CO adsorption peaks in CO-DRIFTS seem independent on the hydrogenation activity and selectivity with PDA increasing, the ratio of $Pt^{\delta+}$ to Pt^0 increase with boosting PDA. $Pt^{\delta+}$ species fraction has a surge over 6wt% PDA catalyst and then slowdown (Table 1). CO-DRIFTS give an evidence that Pt species exist in more types on PDA

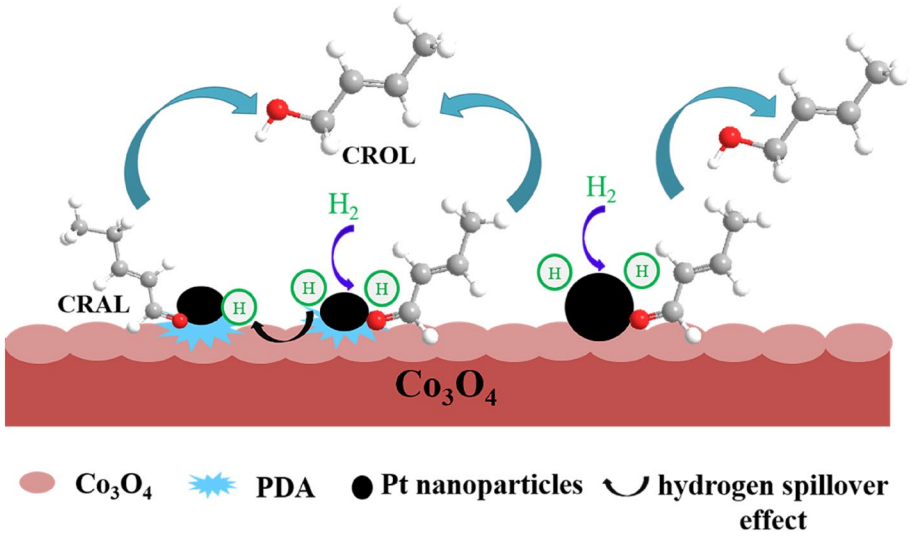

Scheme 2 Proposed the possible reaction pathway of the selective hydrogenation of crotonaldehyde over Pt/Co_3O_4@PDA catalysts

modified catalysts than Pt/Co_3O_4. Actually, the selectivity and yield of 6wt% PDA and 8wt% PDA are similar, which are consistent with the trend of the $Pt^{\delta+}$ species fraction. Furthermore, FT-IR detected the blue shift of $\delta_{N\text{-}H}$ vibration peak over Pt/Co_3O_4@6wt%PDA comparing with Co_3O_4@6wt%PDA, indicating the interaction between Pt and amine changes the electron density of Pt which facilitates the selective hydrogenation of C=O bond.

Based on the above discussion, a possible reaction pathway of the selective hydrogenation of crotonaldehyde over Pt/Co_3O_4@PDA catalysts was outlined. As shown in Scheme 2, the H_2 molecules were activated by metallic Pt species at first. Meanwhile, the Pt-PDA and Pt-Co_3O_4 interface sites adsorbed and activated the C=O bond of crotonaldehyde. More importantly, Pt-PDA can facilitate H_2-spillover effect and then the hydrogenation process was accelerated.

5 Conclusion

In this study, series of Pt/Co_3O_4@PDA catalysts were synthesized by simple method for the selective hydrogenation of crotonaldehyde. Changing the amount of PDA to Co_3O_4 from 4 to 8%, it was found that both of selectivity towards the crotyl alcohol (69.9%) and the formation rate of crotyl alcohol were effectively improved, which mainly due to the synergy of Pt-PDA and Pt-Co_3O_4 dual interface active sites. The control tests and systematic characterizations revealed Pt-PDA and Pt-Co_3O_4 interfaces are favorable to adsorb and activate C=O, meanwhile Pt-PDA can accelerate selective hydrogenation by boosting H_2-spillover effect. In addition, Pt/Co_3O_4@6wt%PDA shows universal selectivity for C=O hydrogenation in other α,β-unsaturated aldehydes to corresponding unsaturated alcohols with high selectivity, such as > 99.9% of furfuryl alcohol and 94% of cinnamyl alcohol. This strategy provides a great prospect for Pt based catalysts towards selective hydrogenation reactions of α,β-unsaturated aldehydes.

Supplementary Information The online version contains supplementary material available at https://doi.org/10.1007/s10562-022-04022-2.

Acknowledgements Financial supports by National Natural Science Foundation of China (21773272) and CAS "Light of West China" Program are gratefully acknowledged.

Declarations

Conflict of interest The authors declare no conflict of interest.

References

1. Song T, Ma Z, Yang Y (2019) ChemCatChem 11:1313–1319
2. Yu J, Yang Y, Chen L, Li Z, Liu W, Xu E, Zhang Y, Hong S, Zhang X, Wei M (2020) Appl Catal B 277:119273
3. Taniya K, Jinno H, Kishida M, Ichihashi Y, Nishiyama S (2012) J Catal 288:84–91
4. Jia A, Zhang Y, Song T, Hu Y, Zheng W, Luo M, Lu J, Huang W (2021) Chin J Catal 42:1742–1754
5. Bai S, Bu L, Shao Q, Zhu X, Huang X (2018) J Am Chem Soc 140:8384–8387
6. Yang Y, Rao D, Chen Y, Dong S, Wang B, Zhang X, Wei M (2018) ACS Catal 8:11749–11760
7. Kahsar KR, Schwartz DK, Medlin JW (2014) J Am Chem Soc 136:520–526
8. Wang W, Xie Y, Zhang S, Liu X, Haruta M, Huang J (2018) Catalysts 8:60–63
9. Yang X, Mueanngern Y, Baker QA, Baker LR (2016) Catal Sci Technol 6:6824–6835
10. Yua Q, Zhang X, Li B, Lua J, Hua G, Jia A, Luo C, Hong Q, Song Y, Luo M (2014) J Mol Catal A 392:89–96
11. Taniya K, Yu CH, Takado H, Hara T, Okemoto A, Horie T, Ichihashi Y, Tsang SC, Nishiyama S (2018) Catal Today 303:241–248

12. Wu JCS, Cheng TS, Lai CL (2006) Appl Catal A 314:233–239
13. Dandekar A, Vannice MA (1999) J Catal 183:344–354
14. Abid M, Paul-Boncour V, Touroude R (2006) Appl Catal A 297:48–59
15. Wang X, He Y, Liu Y, Park J, Liang X (2018) J Catal 366:61–69
16. Sen MAB (1989) J Catal 115:65–78
17. Liberková K, Touroude R (2002) J Mol Catal A 180:221–230
18. Mahata N, Gonçalves F, Pereira MFR, Figueiredo JL (2008) Appl Catal A 399:159–168
19. Tsang SC, Cailuo N, Oduro W, Kong ATS, Clifton L, Yu KMK, Thiebaut B, Cookson J, Bishop P (2008) ACS Nano 2:2547–2553
20. Ning X, Xu YM, Wu AQ, Tang C, Jia AP, Luo MF, Lu JQ (2019) Appl Surf Sci 463:463–473
21. Lin W, Cheng H, Li X, Zhang C, Zhao F, Arai M (2018) Chin J Catal 39:88–996
22. Aoun M, Benamar A, Chater M (2011) Chin J Catal 32:1185–1190
23. Liu Y, Ai K, Lu L (2014) Chem Rev 114:5057–5115
24. Lakra R, Kumar R, Thatoi DN, Sahoo PK, Soam A (2021) Mater Today 41:269–271
25. Zhua X, Feng H, Chen R, Liao Q, Ye D, Zhang B (2019) Appl Surf Sci 487:416–425
26. Bian SW, Liu S, Chang L (2016) J Mater Sci 51:3643–3649
27. Khan MK, Butolia P, Jo H, Irshad M, Han D, Nam KW, Kim J (2020) ACS Catal 10:10325–10338
28. Velu S, Gangwal SK (2006) Solid State Ion 177:803–811
29. Smeds S, Salmi T, Lindfors LP (1996) Appl Catal A 144:177–194
30. Lan X, Wang T (2020) ACS Catal 10:2764–2790
31. Wang X, Liang X, Geng P, Li Q (2020) ACS Catal 10:2395–2412
32. Lin H, Zheng J, Zheng X, Gu Z, Yuan Y, Yang Y (2015) J Catal 330:135–144
33. Ye H, Zhao H, Jiang Y, Liu H, Hou Z (2020) ACS Appl Nano Mater 3:12260–12268
34. Wang Y, Zhuo H, Sun H, Zhang X, Dai X, Luan C, Qin C, Zhao H, Li J, Wang M, Ye JY, Sun SD (2019) ACS Catal 9:442–455
35. Liu M, Tang W, Xie Z, Yu H, Yin H, Xu Y, Zhao S, Zhou S (2017) ACS Catal 7:1583–1591
36. Shiraishi Y, Sakamoto H, Fujiwara K, Ichikawa S, Hirai T (2014) ACS Catal 4:2418–2425
37. Yao C, Xue J, Xu L, Su Y, Bu J, Priestley RD, Hou S (2020) Appl Surf Sci 541:148329
38. Cai A, Wang X, Guo A, Chang Y (2016) J Photochem Photobiol B 162:482–492
39. Song H, Wang Z, Yang J, Jia X, Zhang Z (2017) Chem Eng J 324:51–62
40. Lo WS, Chou LY, Young AP, Ren C, Goh T, Williams BP, Li Y, Chen SY, Ismail MN, Huang W, Tsung CK (2021) Chem Mater 33:1946–1953
41. Yang Q, Li L, Wang X, Ma Y (2022) J Hazard Mater 424:127601
42. Shen M, Lv L, Wang J, Zhu J, Huang Y, Wang J (2014) Chem Eng J 255:40–48
43. Cao Z, Bu J, Zhong Z, Sun C, Zhang Q, Wang J, Chen S, Xie X (2019) Appl Catal A 578:105–115
44. Chakarova K, Mihaylov M, Hadjiivanov K (2005) Micropor Mesopor Mater 81:305–312
45. Kennedy G, Baker LR, Somorjai GA (2014) Angew Chem Int Ed 126:3473–3476
46. Lv Y, Han M, Gong W, Wang D, Chen C, Wang G, Zhang H, Zhao H (2020) Angew Chem Int Ed 59:23521–23526
47. Wu B, Huang H, Yang J, Zheng N, Fu G (2012) Angew Chem Int Ed 51:3440–3443
48. Vu K, Bukhryakov K, Anjum D, Rodionov V (2015) ACS Catal 5:2529–2533
49. Li W, Wang Y, Chen P, Zeng M, Jiang J, Jin Z (2016) Catal Sci Technol 6:7386–7390
50. Han X, Zhou R, Yue B, Zheng X (2006) Catal Lett 109:157–161
51. Plomp AJ, van Asten DMP, van der Eerden AMJ, Mäki-Arvela P, Murzin DY, de Jong KP, Bitter JH (2009) J Catal 263:146–154
52. Concepción P, Corma A, Silvestre-Albero J, Franco V, Chane-Ching JY (2004) J Am Chem Soc 126:5523–5532
53. Ruppert AM, Paryjczak T (2007) Appl Catal A 320:80–90
54. Englisch M, Jentys A, Lercher J (1997) J Catal 166:25–35
55. Zhu Y, Zaera F (2014) Catal Sci Technol 4:955–962
56. Zhang S, Xia Z, Zhang M, Zou Y, Shen H, Li J, Chen X, Qu Y (2021) Appl Catal B 297:120418